AIChE

Effect of Diluents on Rapid Phase Transition of Water Induced by Combustion

Almerinda Di Benedetto, Francesco Cammarota, Valeria Di Sarli, and Ernesto Salzano
Istituto di Ricerche sulla Combustione, CNR, 80124 Napoli, Italy

Gennaro Russo
Dipt. di Ingegneria Chimica, Università degli Studi di Napoli Federico II, Piazzale Tecchio 80, 80125 Napoli, Italy

DOI 10.1002/aic.12778
Published online November 7, 2011 in Wiley Online Library (wileyonlinelibrary.com).

When exploding $CH_4/O_2/N_2$ mixtures with high oxygen contents in a nonadiabatic vessel, the pressure–time histories display oscillations of different frequencies and very high pressure peaks (hundreds of bars). We have attributed this anomalous behavior (combustion-induced rapid phase transition, cRPT) to the occurrence of cycles of condensation/evaporation of water at the vessel walls, followed by superheating of the liquid film due to radiative heat transfer from the flame, which culminates in the water rapid phase transition. We now report a detailed analysis of the role played by the addition of a diluent (CO_2, N_2, He, and Ar) on the anomalous behavior. The limit values of the diluent concentration at which the cRPT phenomenon is suppressed have been found and correlated to the kinematic viscosity and the thermal diffusivity through the Prandtl number. The less effective diluent has been found to be Ar followed by He, N_2, and CO_2 in the order listed. © 2011 American Institute of Chemical Engineers *AIChE J*, 58: 2810–2819, 2012
Keywords: rapid phase transition, methane combustion, water explosion, diluent, Prandtl number

Introduction

Oxidation or partial oxidation reactions involving hydrocarbons and/or hydrogen are present in most of the chemical processes. Typical processes are syngas production (steam reforming and partial oxidation), ethylene and ethylene oxide production, combustion, and oxy combustion. Such processes all utilize air or oxygen as the oxidant.

Nevertheless, oxidation is one of the most hazardous chemical processes, owing to its potential to undergo uncontrolled combustion such as deflagration and detonation.

Deflagration causes a fast increase of pressure up to the thermodynamic value (≈8 bar), eventually leading to the rupture of the reactor.

Under certain conditions, combustion may transit to a detonation mode giving rise to pressure higher than the thermodynamic value (≈40 bar).

To avoid the dramatic consequences of deflagration and also detonation, a great effort is continuously devoted to the identification of ranges of operating conditions that lead to such combustion modes.

Recently, we have discovered a combustion mode, which has been named combustion-induced rapid phase transition (cRPT).[1] More precisely, we found that $CH_4/O_2/N_2$ mixtures may exhibit exceptional and anomalous behavior, when exploding at extreme concentration conditions in a no adiabatic vessel. Explosion tests were performed in a 5-L vessel for $CH_4/O_2/N_2$ mixtures with stoichiometric CH_4/O_2 ratio, changing the oxygen air enrichment factor, $E = O_2/(O_2 + N_2)$, from 0.21 (air) up to 1 (pure oxygen). We have found that at $E \geq 0.4$, the pressure temporal trend starts oscillating, eventually culminating in very high peaks (up to 400 bar) largely exceeding the adiabatic values. We have attributed the oscillating behavior to the occurrence of cycles of condensation and vaporization at the vessel walls of the water produced by combustion. Such cycles culminate in the superheating and then in the explosive vaporization (i.e., the rapid phase transition) of the water, with the formation of shock waves that lead to overadiabatic pressure peaks.

Explosive vaporization occurs when a liquid reaches its boiling point in the absence of nucleation sites.[2] In such conditions, the boiling process may be delayed and the liquid starts superheating without boiling. When a limit temperature is reached (superheating temperature), homogeneous nucleation occurs spontaneously and the liquid starts boiling in an explosive manner. Such explosion is a physical explosion that is termed rapid phase transition.[2–10] The consequent rapid production of high-pressure vapor exerts sudden pressure on the surrounding fluid, thus leading to the formation of strong shock waves.[11,12] Superheated liquid explosions have been observed in the concomitance to vessel ruptures, in nuclear or foundry accidents, and to volcano eruptions.[11,13–16]

The cRPT is a phenomenon localized at the vessel walls that spreads over the entire vessel, leading to strong overpressures. Indeed, a significant temperature gradient is established across the boundary layer between the wall temperature (10°C) and the bulk gas temperature (∼2500°C). This temperature gradient drives the condensation of the water

Correspondence concerning this article should be addressed to A. Di Benedetto at dibenede@irc.cnr.it.

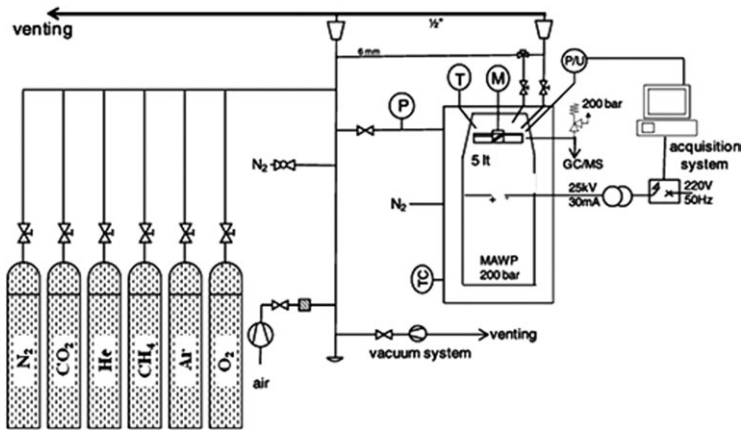

Figure 1. Sketch of the experimental rig.

produced by combustion, when the partial pressure is much higher than the vapor pressure at 10°C, and the evaporation of the liquid water stored in the boundary layer, due to the superheating caused by the heat transferred from the bulk gas phase.

In the literature, similar phenomena for methane/O_2/N_2 and propene/O_2/N_2 mixtures have been observed by Schildberg and Holtappels[17] and Schildberg.[18] They found that as the oxygen concentration increases, not only the transition from deflagration to detonation occurs but also the transition to a combustion regime they called transitional state. The authors conclude that the nature of this transitional state has yet to be clarified. This state exhibits the same features (oscillating pressure–time histories with overadiabatic peaks) as the cRPT phenomenon. The identification and the characterization of the cRPT phenomenon thus represent a starting point for contributing to clarify the nature of severe combustion modes other than classical detonation modes.

In this work, we study the occurrence of the cRPT phenomenon changing the mixture reactivity (i.e., the flame speed) and adiabatic temperature and pressure by adding diluents. We performed explosion tests adding different amounts of CO_2 (ranging from 0 up to 66%). We also substituted CO_2 with diluents having different physical properties such as N_2, Ar, and He.

Experimental

The experimental system has been described recently[1,19] and is just briefly mentioned here for ready reference. The reactor consists of a closed cylindrical vessel made of 5-cm-thick AISI 316 SS steel. The vessel volume is 5 L. Figure 1 shows the scheme of the experimental rig. The reactor is equipped with rupture disks able to stand 200 bar.

Mixtures were obtained by using the partial pressure methodology. After vacuum, the combustion vessel was filled by injecting one mixture component (purity above 99.9% v/v) at time up to reach the specific partial pressure. Gases were premixed by mechanical stirring (rotating shaft velocity equal to 200 rpm). They were allowed to settle for around 30 s and then ignited by an electric spark (25 kV, 30 mA) positioned at the center of the vessel.

For the pressure recording, which is the core measurement for the experiments reported in this article, KULITE ETS-IA-375 (M) series pressure transducers with a natural frequency of 150 kHz were used. These transducers are specifically designed for high pressure, high shock environment, and blast analysis. To avoid any resonance and other side effects of the circuitry, they were fed by continuous current produced by a chemical battery (Winner, 12 VDC and 7 Ah). By this way, 50 Hz effects derived from general supply were avoided, and no AC current was used in any part of the circuitry. No smoothing or filters were used in the electronic circuitry. The full frequency of the Kulite transducer was directly recorded through a National Instrument USB-6251 Data Acquisition System (16 bit, 1.25 M samples/s) hence having a frequency much higher than the transducer, so that no overlapping was possible.

Each test was performed three times, and minimal variations between runs were found. For all tests, the initial pressure was set to 1 bar and the initial temperature to 300 K. The temperature of the vessel walls was equal to the ambient temperature (293 K).

In Table 1, the compositions of the mixtures investigated are reported for different contents of diluents and oxygen air enrichment factors, $E = O_2/(O_2 + N_2)$. For each mixture, Table 1 also gives the maximum theoretical values of pressure (P_{ad}) and temperature (T_{ad}) corresponding to the adiabatic values, and the partial pressure of the water produced (P_{H_2O}) was calculated at adiabatic conditions. Furthermore, the dilution factor (D) is reported in Table 1 as calculated according to

$$D = \frac{\mathrm{Ar} + \mathrm{He} + \mathrm{CO_2} + \mathrm{N_2}}{\mathrm{O_2} + \mathrm{CH_4} + \mathrm{Ar} + \mathrm{He} + \mathrm{CO_2} + \mathrm{N_2}} \quad (1)$$

Theory: Characteristic Times

In our previous article,[1] to get insights into the nature of the oscillations and overadiabatic peaks, we compared the periods of the oscillating pressure histories with the time constants of all the processes involved. To compute the period of the oscillations, fast Fourier transform (FFT) analysis of the pressure time signals was performed.

The time constants were evaluated for chemical, gasdynamic, and reactor-related processes. In Tables 1 and 2, the values of parameters and physical/chemical properties used for such evaluations are given.

The reaction time, τ_{reac}, was calculated considering the time required by the flame to travel along the radial direction of the vessel

$$\tau_{reac} = \frac{d/2}{S_F} \quad (2)$$

Table 1. Mixture Composition, Adiabatic Pressure and Temperature, and Partial Pressure of the Water Produced as Calculated at Adiabatic Conditions, Laminar Burning Velocity, Speed of Sound, and Emissivity

RUN	CH_4 (%)	O_2 (%)	N_2 (%)	CO_2 (%)	He (%)	Ar (%)	D (%)	P_{ad} (bar)	T_{ad} (K)	P_{H_2O} (bar)	S_l (m/s)	$C_{unburned}$ (m/s)	C_{burned} (m/s)	ε
1	7.3	14.5	58.2	20.0	0	0	78.0	6.9	2072	1.0	0.07	331	828	0.12
2	13.3	26.7	40.0	20.0	0	0	60.0	9.3	2693	2.3	0.50	332	957	0.10
3	18.5	36.9	24.6	20.0	0	0	45.0	10.7	2962	3.3	0.95	333	1026	0.10
4	22.9	45.7	11.4	20.0	0	0	31.0	11.7	3123	4.1	1.45	333	1076	0.09
5	26.7	53.3	0	20.0	0	0	20.0	12.6	3239	4.8	1.10	333	1118	0.10
6	17.0	34.0	9.0	40.0	0	0	49.0	9.7	2757	2.9	0.56	313	925	0.11
7	19.0	37.0	9.0	35.0	0	0	44.0	10.3	2868	3.3	0.73	321	981	0.11
8	20.0	40.0	10.0	30.0	0	0	40.0	10.7	2950	3.5	0.94	323	999	0.10
9	21.0	43.0	11.0	25.0	0	0	36.0	11.2	3033	3.8	1.20	325	1021	0.10
10	23.0	46.0	11.0	20.0	0	0	31.0	11.7	3126	4.1	1.45	333	1076	0.09
11	28.6	57.1	14.3	0	0	0	14.3	14.7	3444	5.2	2.73	356	1248	0.08
12	18.5	36.9	24.6	20.0	0	0	44.6	10.7	2962	3.3	0.98	327	1026	0.09
13	18.5	36.9	0	20.0	24.6	0	44.6	11.1	3040	3.3	1.17	375	1178	0.10
14	18.5	36.9	0	20.0	0	24.6	44.6	11.1	3041	3.3	1.07	321	1009	0.09
15	18.5	36.9	0	44.6	0	0	44.6	10.0	2803	3.4	0.50	310	925	0.11
16	18.5	36.9	44.6	0	0	0	44.6	11.5	3160	3.2	1.54	355	1136	0.08
17	18.5	36.9	0	0	44.6	0	44.6	12.4	3320	3.1	2.12	468	1552	0.07
18	18.5	36.9	0	0	0	44.6	44.6	12.4	3320	3.1	1.86	333	1105	0.07
19	13.3	26.7	0	0	60.0	0	60.0	11.3	3171	2.2	1.55	533	1693	0.06
20	11.7	23.3	0	0	65.0	0	65.0	10.9	3105	2.0	1.32	564	1765	0.06
21	10.0	20.0	0	0	70.0	0	70.0	10.5	3018	1.7	1.06	594	1825	0.06
22	15.0	30.0	55.0	0	0	0	55.0	10.6	3004	2.6	1.10	354	1098	0.07
23	13.0	26.6	60.0	0	0	0	60.0	10.0	2896	2.2	0.88	354	1060	0.07
24	11.7	23.3	65.0	0	0	0	65.0	9.6	2790	2.0	0.66	354	1037	0.07
25	20.0	40.0	0	40.0	0	0	40.0	10.5	2892	3.5	0.78	314	959	0.10
26	19.2	38.3	0	42.5	0	0	42.5	10.2	2845	3.4	0.68	311	940	0.10
27	18.5	36.9	0	44.6	0	0	44.6	10.0	2802	3.2	0.60	310	925	0.11
28	11.7	23.3	0	0	0	65.0	65.0	10.9	3104	2.0	1.06	327	1024	0.06
29	10.0	20.0	0	0	0	70.0	70.0	10.5	3018	1.7	0.84	326	1001	0.06
30	9.2	18.3	0	0	0	72.5	72.5	10.2	2966	1.5	0.71	325	988	0.06

where d is the reactor diameter, and S_F is the flame speed calculated as a function of the laminar burning velocity, S_l, and the expansion factor (i.e., the adiabatic pressure, P_{ad}, to initial pressure, P^o, ratio)

$$S_F = S_l \cdot E = S_l \cdot (P_{ad}/P^o) \tag{3}$$

In Eq. 3, the expansion factor was evaluated assuming all gas as burned and at the maximum theoretical pressure (P_{ad}).

The explosion phenomenon is unsteady and dominated by the thermal inertia of the vessel walls. It is then interesting to evaluate the heating/cooling time of the vessel walls, τ_{hcw}

$$\tau_{hcw} = \frac{{\delta_w}^2}{\alpha_w} \tag{4}$$

where δ_w is the wall thickness (0.05 m) and α_w is the wall thermal diffusivity (4.54×10^{-5} m^2/s). τ_{hcw} is equal to about 55 s. This time is much higher than the explosion time ($\approx$100 ms). As a consequence, during the unsteady pressure increase due to explosion, the vessel walls behave as isothermal walls with $T_w \approx 10$°C.

Notwithstanding, the combustion process is not adiabatic. Besides heat losses by natural convection, the flame exchanges heat with the vessel walls through radiation. The time of heat exchange between flame and walls by radiation, τ_{rad}, was computed through the following formula

$$\tau_{rad} = \frac{\rho C_p V (T_F - T_w)}{\sigma \varepsilon A ({T_F}^4 - {T_w}^4)} \tag{5}$$

where ρ and C_p are the gas density and specific heat capacity, V the vessel volume, T_F the flame temperature (adiabatic temperature), σ the Stefan–Boltzmann constant, ε the emissivity, and A the surface area enclosing the radiating gas volume (assumed as equal to the surface area of the vessel walls).

The combustion-generated pressure waves travel along the reactor. The time of pressure wave propagation, τ_w, was calculated according to

$$\tau_w = \frac{L}{c} \tag{6}$$

where L is the reactor length and c is the sound speed.

The combustion reaction produces water whose adiabatic partial pressure is given in Table 1. Depending on the relative values of the water partial pressure and the water vapor pressure at 10°C (temperature of the vessel walls), which is equal to 0.02 bar, condensation may occur at the walls. The condensation time, τ_{cond}, was then calculated as

$$\tau_{cond} = \frac{\rho C_p V}{h_c S} \tag{7}$$

Table 2. Values of Parameters and Physical/Chemical Properties Used for Evaluating the Characteristic Times

Parameter	Symbol	Value
Gas specific heat capacity	C_p (J/kg K)	Calculated at T_{ad} (burned mixture)
Gas density	ρ (kg/m^3)	Ideal gas equation (burned mixture)
Gas thermal diffusivity	α (m^2/s)	2×10^{-5}
Laminar burning velocity	S_l (m/s)	See Table 1
Flame speed	S_F (m/s)	S_l^* (P_{ad}/P°)
Speed of sound at T_{ad}	c (m/s)	See Table 1
Reactor length	L (m)	0.4
Reactor internal diameter	d (m)	0.14

Table 3. Characteristic Times, Time of Pressure Peak, Peak Pressure, Peak Severity, and Periods of the Oscillations

RUN	Behavior	τ_{reac} (ms)	τ_{rad} (ms)	τ_{cond} (ms)	τ_w (ms)	θ_1	θ_2	t_{peak} (cRPT) (ms)	P_{peak} (cRPT)	K_{Crpt} (bar m/s)	T_I (ms)	T_II (ms)	T_III (ms)
1	Under	144.0	32.7	12.2	0.5	0.08	0.37	–	–	–	–	–	–
2	Under	68.3	16.5	11.7	0.5	0.17	0.71	–	–	–	–	–	–
3	Over	6.9	13.7	11.9	0.4	1.72	0.87	42.3	28	9582	0.7	1.1	1.3
4	Over	4.1	11.7	11.9	0.4	2.89	1.02	11.0	181	124,110	0.4	1.1	0.8
5	Over	5.0	10.9	11.3	0.4	2.24	1.04	10.3	76	64,948	0.7	0.8	1.3
6	Under	12.9	14.6	12.3	0.4	0.95	0.84	–	–	–	–	–	
7	Over	9.3	13.7	12.3	0.4	1.30	0.90	62.1	27	31,450	0.8	1.4	1.3
8	Over	6.9	1.3	12.3	0.4	1.70	9.20	41.2	54	29,846	0.7	1.7	1.7
9	Over	5.1	12.4	12.0	0.4	2.30	0.96	32.3	49	55,490	0.3	1.1	1.3
10	Over	4.1	11.9	11.9	0.4	2.90	1.00	11.0	181	124,110	0.4	1.7	0.8
11	Over	1.9	10.8	11.4	0.3	6.10	1.06	2.4	282	1,609,242	/	/	1.3
12	Over	6.7	12.4	11.7	0.4	1.76	0.95	39.4	28	31,942	0.2	0.8	1.1
13	Over	5.4	9.9	11.0	0.3	2.04	1.11	38.1	80	274,722	0.4	1.1	1.3
14	Over	6.3	10.5	11.0	0.4	1.75	1.05	28.7	42	111,058	0.4	1.0	1.2
15	Under	14.0	13.2	12.4	0.4	0.79	0.94	–	–	–	–	–	–
16	Over	4.0	10.3	11.1	0.3	3.14	1.08	106.0	49	56,058	0.6	0.8	1.1
17	Over	2.7	8.0	9.8	0.3	4.69	1.23	8.1	146	832,974	0.5	0.8	0.8
18	Over	2.7	10.1	12.5	0.3	3.68	1.23	8.5	110	2,216,822	0.4	1.1	1.2
19	Over	4.0	10.0	9.3	0.2	2.32	0.92	49.6	400	14,928	0.2	1.4	1.3
20	Over	4.8	10.6	9.1	0.2	1.87	0.86	75.9	12	250	0.2	1.4	1.1
21	Under	6.3	11.4	8.8	0.2	1.41	0.77	–	–	–	–	–	–
22	Over	6.0	13.1	11.1	0.4	1.84	0.85	77.6	249	102,398	0.4	1.4	2.2
23	Under	8.0	14.3	11.1	0.4	1.39	0.78	–	–	–	–	–	–
24	Under	11.1	15.8	10.7	0.4	0.96	0.67	–	–	–	–	–	–
25	Over	8.6	12.7	12.4	0.4	1.45	0.98	97.4	204	90,678	0.8	1.5	0.7
26	Over	10.0	13.8	12.5	0.4	1.25	0.90	122.0	72	16,444	0.7	2.5	1.0
27	Under	11.6	13.6	12.5	0.4	1.08	0.92	–	–	–	–	–	–
28	Over	6.0	12.1	8.8	0.4	1.46	0.73	85.0	59	83,936	0.4	2.0	0.8
29	Over	8.0	13.3	8.8	0.4	1.11	0.66	130.0	14	2026	0.3	2.8	1.1
30	Under	9.6	14.0	8.7	0.4	0.91	0.62	–	–	–	–	–	–

where h_c is the coefficient of heat transfer due to condensation at the walls evaluated according to the formula reported by Incropera and DeWitt,[20] and S is the internal surface of the vessel.

We also calculated the ratio between the condensation time (τ_{cond}) and the time for radial flame propagation (τ_{reac}), θ_1

$$\theta_1 = \frac{\tau_{cond}}{\tau_{reac}} \tag{8}$$

and the ratio between the condensation time (τ_{cond}) and the flame radiation time (τ_{rad}), θ_2

$$\theta_2 = \frac{\tau_{cond}}{\tau_{rad}} \tag{9}$$

In Table 1, the values of the laminar burning velocity (S_l) and the sound speed in the unburned ($c_{unburned}$) and burned (c_{burned}) gases are given. The values of S_l were computed by means of the Premix module of the CHEMKIN software.[21]

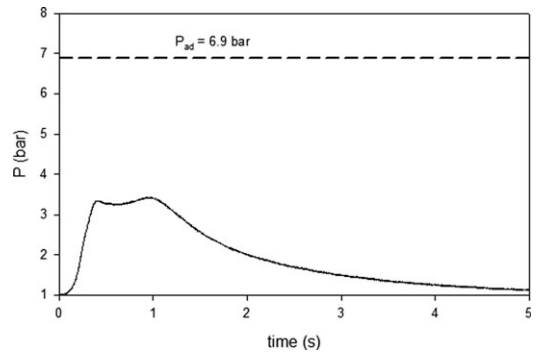

Figure 2. Pressure vs. time for RUN 1 (dashed line: adiabatic pressure).

In Table 1, the emissivity of the burned mixtures is also reported as computed by means of the formula proposed by Leckner,[22] which has been widely tested for $CO_2/H_2O/N_2$ mixtures.

In Table 3, the values of the time constants are given.

Combustion-Induced Rapid Phase Transition

In Figure 2, the pressure–time history obtained for $E = O_2/(O_2 + N_2) = 0.21$ and $CO_2 = 20\%$ (RUN 1) is shown. The adiabatic pressure value is also reported (dashed line).

The differences between the peak pressure (3.4 bar) and the adiabatic pressure (6.9 bar) can be attributed to heat losses and also to the condensation of the water produced

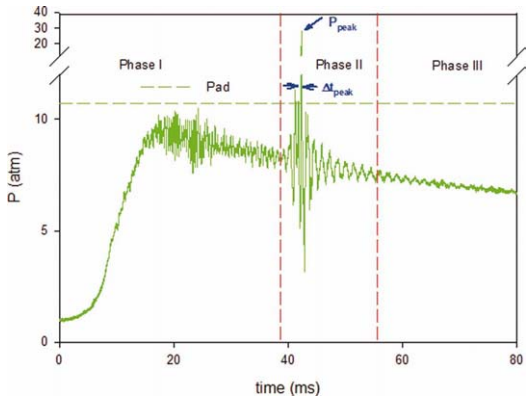

Figure 3. Pressure vs. time for RUN 3 with phase identification (dashed line: adiabatic pressure).

[Color figure can be viewed in the online issue, which is available at wileyonlinelibrary.com.]

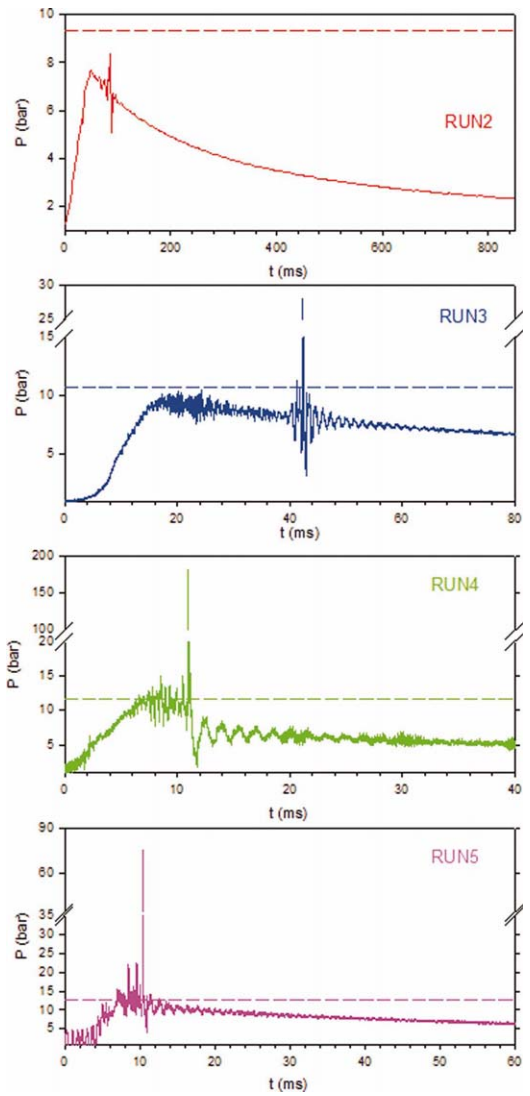

Figure 4. Pressure vs. time for different oxygen air enrichment factors (CO_2 = 20%): RUN 2–5.

[Color figure can be viewed in the online issue, which is available at wileyonlinelibrary.com.]

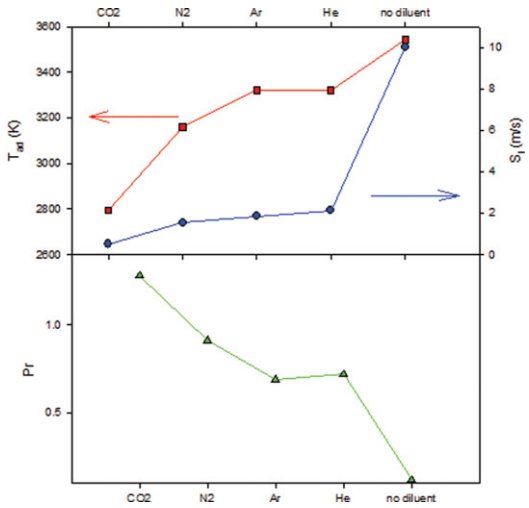

Figure 5. Computed laminar burning velocity and adiabatic temperature (top) and Prandlt number (bottom) for CH_4/O_2/d mixtures with d = CO_2, N_2, Ar, and He (D = 44.6%).

[Color figure can be viewed in the online issue, which is available at wileyonlinelibrary.com.]

during combustion. Indeed, the water condensation at the vessel walls causes a reduction of the maximum pressure (equal to the water partial pressure, P_{H_2O} = 1 bar, Table 1) with respect to the adiabatic pressure and also further cooling of the burned gases.

When increasing the oxygen content in the mixture (E = 0.6, RUN 3), we find that the pressure signal changes both quantitatively and qualitatively (Figure 3). The features of the pressure trend are completely different from those found with RUN 1 (Figure 2). More precisely, the pressure signal starts oscillating and also the peak pressure (P_{peak} = 28 bar) is much higher than the adiabatic value (P_{ad} = 10.7 bar).

In a previous article, we have named such anomalous behavior as cRPT.[1] We have attributed the oscillating behavior to the occurrence of cycles of condensation and vaporization (at the vessel walls) of the water produced during the flame propagation. Such cycles culminate in the rapid phase transition of the condensed water, leading to the overadiabatic pressure peak.

As shown in Figure 3, the pressure trend can be divided into three parts, which correspond to different phases of the chemical/physical processes occurring in the vessel.

Phase I is characterized by the typical trend of closed-vessel chemical explosions: the average pressure increases up to the adiabatic value ($P_{ad} \sim$ 10.7 bar). The maximum (adiabatic) pressure is achieved at an elapsed time after ignition that corresponds to the time required by the laminar flame to propagate along the entire length of the vessel, $t \approx$ 19 ms. At this time, we may assume that the combustion reaction is completed. After this time, the pressure starts decreasing due to the effect of heat losses.

Surprisingly, the pressure signal is an oscillating signal, and the oscillation amplitude increases with time up to the overadiabatic peak encountered in phase II. It is worth emphasizing that this peak appears when the combustion reaction has come to an end. The pressure decrease of the last phase (III) is due to heat losses.

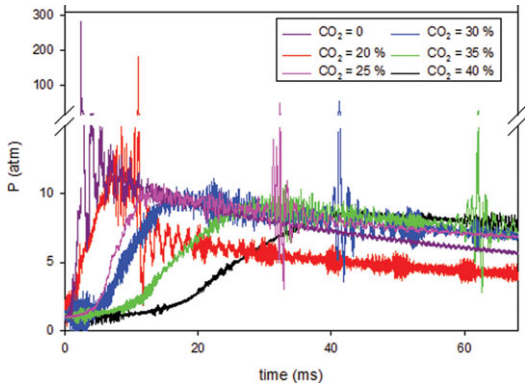

Figure 6. Pressure vs. time for $CH_4/O_2/N_2/CO_2$ mixtures with different CO_2 contents (RUN 6–11).

[Color figure can be viewed in the online issue, which is available at wileyonlinelibrary.com.]

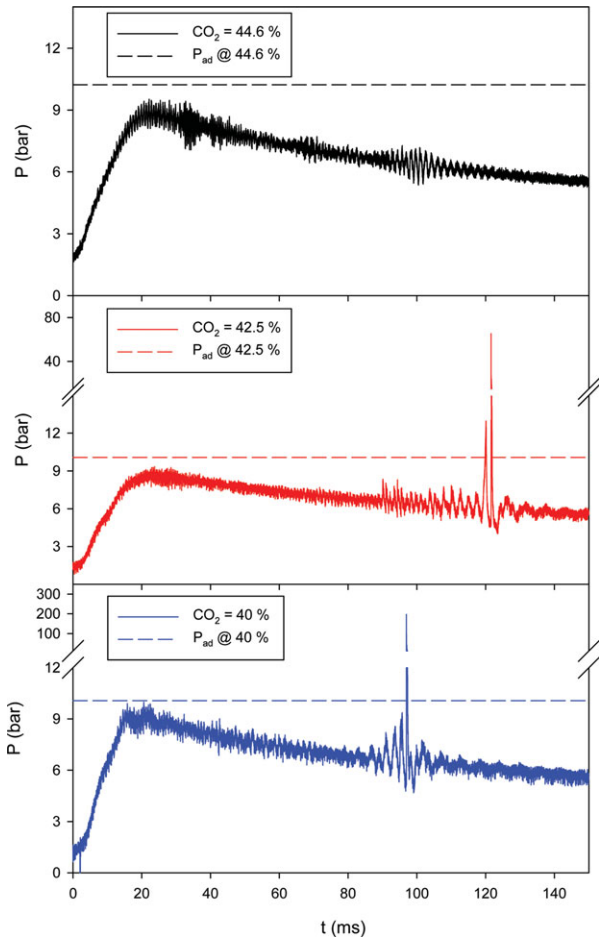

Figure 7. Pressure vs. time for $CH_4/O_2/CO_2$ mixtures with different CO_2 contents (RUN 25–27).

[Color figure can be viewed in the online issue, which is available at wileyonlinelibrary.com.]

For each run, we measured the peak pressure corresponding to the value of the cRPT peak (P_{peak}) and the time at which the cRPT peak pressure occurs (t_{peak}). We calculated the severity of the cRPT phenomenon by means of the deflagration index (K_{cRPT})

$$K_{cRPT} = [P_{peak}/(\Delta t_{peak}/2)]V^{1/3} \quad (10)$$

where Δt_{peak} is the time interval of peak duration, and V is the vessel volume. In Table 3, the values of P_{peak}, t_{peak}, and K_{cRPT} are given.

Results

Effect of enriching air with oxygen

In Figure 4, the pressure–time histories are shown as obtained for different oxygen air enrichment factors, E (RUN 2–5). With RUN 2 (O_2 = 26.7%), the cRPT phenomenon does not occur. It occurs with RUN 3, RUN 4, and RUN 5 (O_2 = 36.9, 45.7, and 53.3%). The pressure peak occurs earlier with increasing oxygen content. It is noting that in RUN 2, a peak pressure is observed even if it is not overadiabatic (or overthermodynamic) after the maximum pressure. This peak could still be addressed to the occurrence of water rapid phase transition.

The results of Figure 4 show that on increasing the strength of the mixture (increase of the reactant concentration or decrease of the nitrogen content), the violence of the cRPT phenomenon significantly increases. We then investigated the role diluents in terms of concentration and nature.

Effects of diluents

We studied the cRPT phenomenon by adding different amounts of CO_2 to mixtures with a fixed value of the oxygen air enrichment factor. The qualitative effects are studied substituting CO_2 with N_2, He, and Ar, once fixed the total diluent amount (D = 44.6%).

In Figure 5, the laminar burning velocities are shown as computed for CH_4/O_2/d mixtures (d = CO_2, N_2, He, and Ar) by means of the CHEMKIN software[21] coupled to the GriMech 3.1 mechanism.[23] The adiabatic temperatures are also reported in the figure.

On the bottom graph of Figure 5, the Prandtl number (i.e., the ratio between the kinematic viscosity and the thermal diffusivity) is shown. It is worth noting that kinetics (laminar burning velocity) and thermodynamics (adiabatic temperature) exhibit a monotonic trend when ranging from CO_2 to no diluents. On the contrary, the Pr number exhibits a local maximum with He.

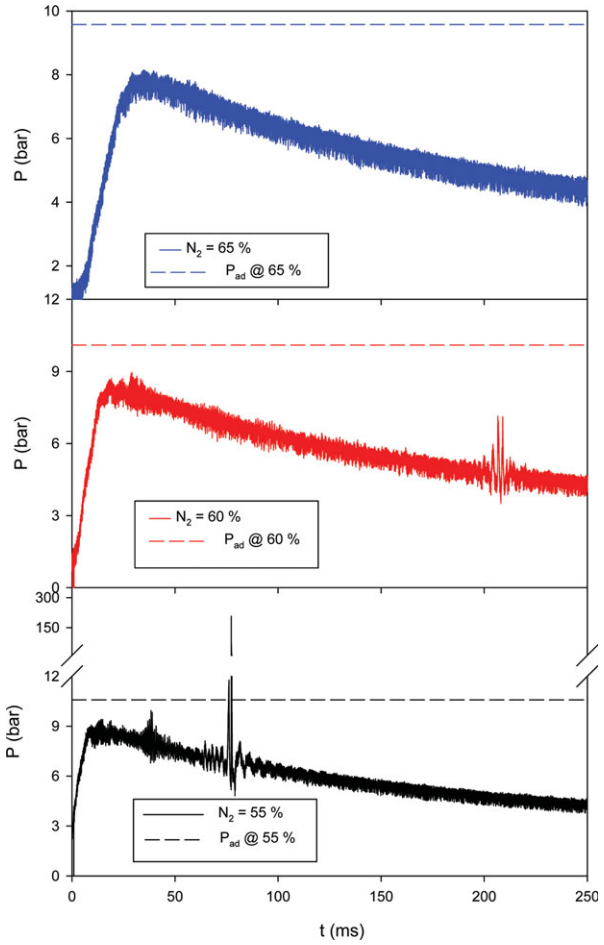

Figure 8. Pressure vs. time for $CH_4/O_2/N_2$ mixtures with different N_2 contents (RUN 22–24).

[Color figure can be viewed in the online issue, which is available at wileyonlinelibrary.com.]

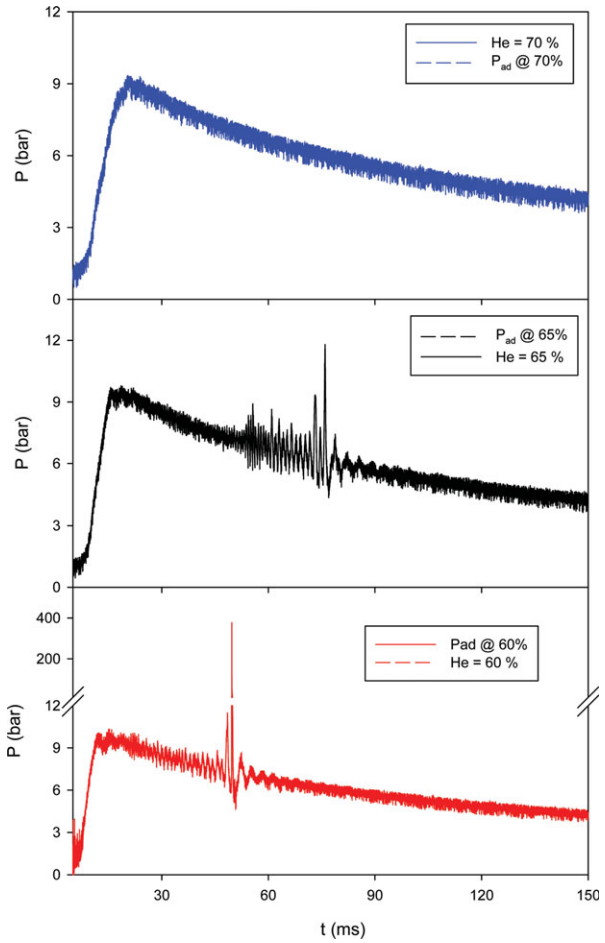

Figure 9. Pressure vs. time for CH_4/O_2/He mixtures with different He contents (RUN 19–21).

[Color figure can be viewed in the online issue, which is available at wileyonlinelibrary.com.]

Effect of diluent concentration

In Figure 6, the pressure–time histories of $CH_4/O_2/N_2/CO_2$ mixtures are shown for different CO_2 contents and then dilution amounts, D (RUN 6–11).

It is found that, for CO_2 content equal to 40% (D = 49%), the pressure does not exhibit an overadiabatic peak (dark line). It takes about 50 ms to reach the adiabatic pressure (9.7 bar) and then starts decreasing due to heat losses. As the diluent amount decreases, a transition from an underadiabatic behavior to an overadiabatic behavior is observed: for CO_2 content equal to 35% (D = 44%; green line), the peak pressure is equal to 27.5 bar and reaches the value of 282 bar for CO_2 = 0% (D = 14.3%; violet line). In all cases with the cRPT phenomenon, the pressure signals oscillate during the transient phase.

Effect of diluent nature

In Figure 7, the pressure–time histories are shown as obtained for $CH_4/O_2/CO_2$ mixtures with different CO_2 contents (RUN 25–27). The adiabatic pressure values are also reported in the figure (dashed lines). On increasing the CO_2 content, the cRPT peak pressure decreases. In addition, the peak shifts at higher times and disappears for CO_2 content equal to 44.6%.

In Figure 8, the pressure–time histories are shown as obtained for $CH_4/O_2/N_2$ mixtures with different N_2 contents (RUN 22–24). The adiabatic pressure values are also reported. No cRPT is found for N_2 contents equal to 65 and 60%. The cRPT phenomenon occurs for N_2 content equal to 55%.

In Figure 9, the pressure–time histories obtained adding He to CH_4/O_2 mixtures (RUN 19–21) are shown together with the corresponding values of adiabatic pressure. In the presence of 60% He, a cRPT peak equal to about 400 bar is attained. As the He content increases, the peak disappears (He content equal to 65 and 70%).

In Figure 10, the pressure temporal trends obtained adding Ar to CH_4/O_2 mixtures are shown (RUN 28–30). When increasing the Ar content from 60 to 70%, the cRPT peak

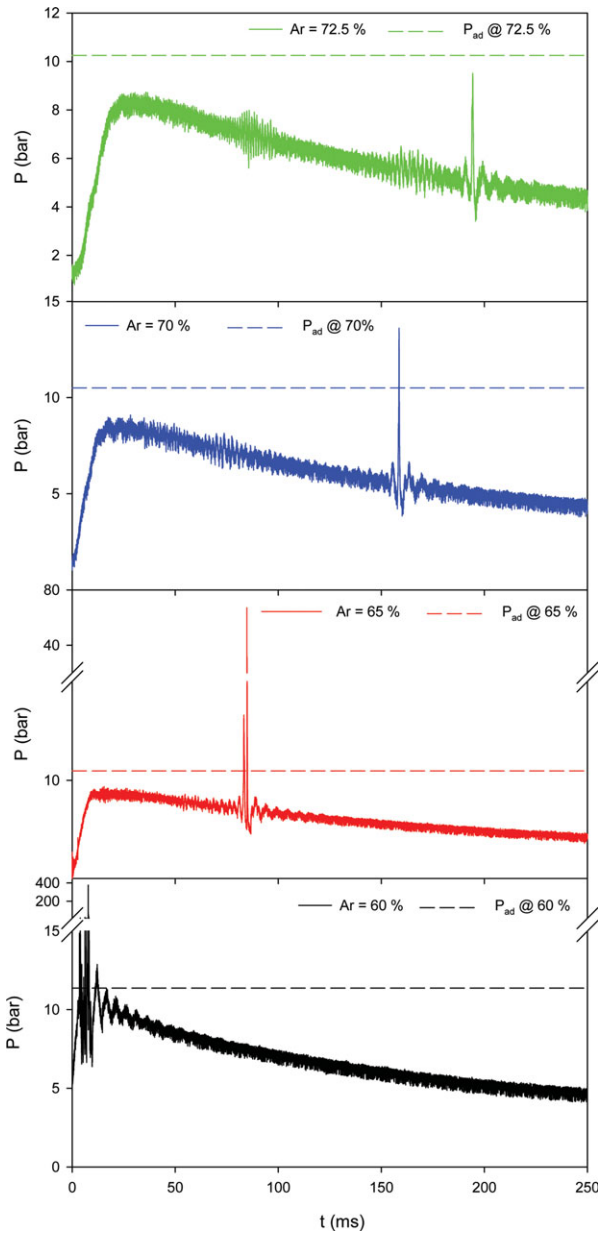

Figure 10. Pressure vs. time for CH_4/O_2/Ar mixtures with different Ar contents (RUN 28–30).

[Color figure can be viewed in the online issue, which is available at wileyonlinelibrary.com.]

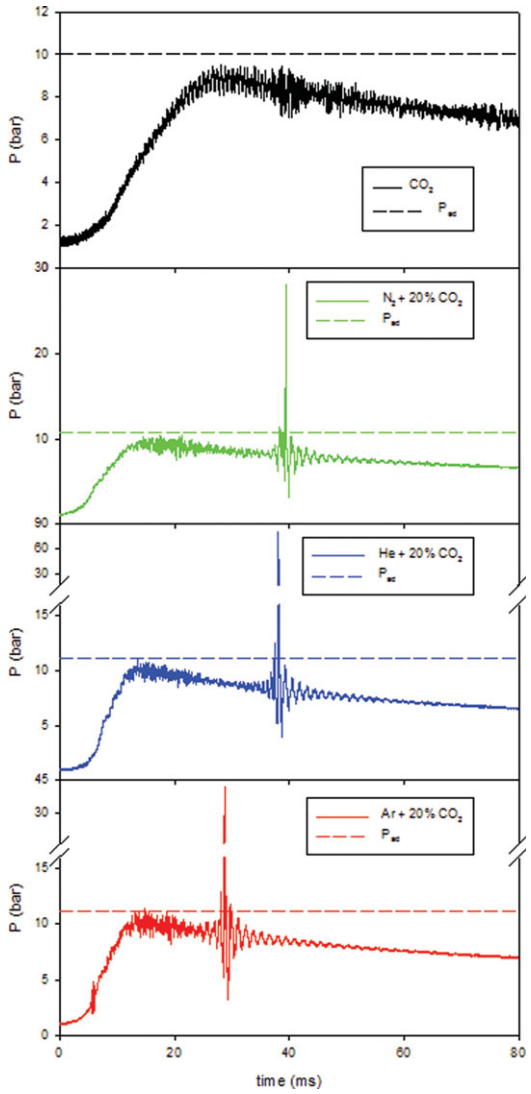

Figure 11. Pressure vs. time for $CH_4/O_2/CO_2$/d mixtures obtained substituting part (24.6%) of the CO_2 content with d = N_2, He, and Ar (RUN 12–15).

[Color figure can be viewed in the online issue, which is available at wileyonlinelibrary.com.]

delays and the peak pressure decreases. The peak disappears for Ar content equal to 72.5%.

Comparison between diluents

From the above results, it turns out that CO_2 is the diluent that allows the most effective suppression of the cRPT phenomenon. We then used CO_2 as the reference diluent and studied the cRPT phenomenon by progressively substituting CO_2 with d = N_2, He, and Ar. In particular, we started from $CH_4/O_2/CO_2$ mixture with CO_2 content equal to 44.6%, for which the occurrence of cRPT is not found (Figure 7), and then progressively substituted CO_2 with different diluents. In Figure 11, the pressure histories for $CH_4/O_2/CO_2$/d mixtures are shown as obtained substituting part (24.6%) of the CO_2 content with *d* (RUN 12–15).

Only in the presence of CO_2, the cRPT phenomenon does not occur. When substituting part of the CO_2 content with N_2, Ar, and He, the cRPT phenomenon is observed. In going from N_2 to Ar and to He, the peak pressure becomes stronger.

When substituting all the CO_2 content (44.6%) with *d* (RUN 16–18), the cRPT phenomenon becomes much more severe, giving rise to peak pressures of hundred bars (Figure 12).

The above discussed results show that the occurrence of the cRPT phenomenon and its violence are strongly affected by both concentration and nature of the diluent. From the data obtained, it is possible to derive the minimum content of diluent (D_cRPT limit) for avoiding the occurrence of the cRPT phenomenon. In Figure 13, the D_cRPT limits are plotted vs. the *Pr* number for all the diluents.

The points in Figure 13 represent the D_cRPT limits that allow us to delimit two zones: for diluent content higher than D_cRPT limit, the cRPT occurrence is prevented; for diluent content lower than D_cRPT limit, the cRPT phenomenon is triggered.

We found that the D_cRPT limits depend on the Prandtl number. In Figure 13, the line corresponds to the theoretical correlation between D_cRPT limit and *Pr*

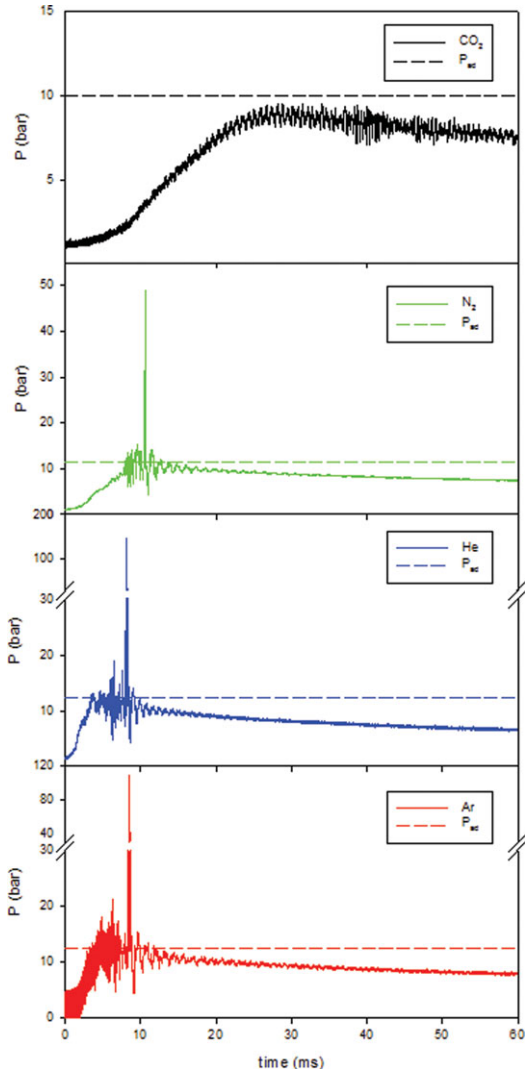

Figure 12. Pressure vs. time for $CH_4/O_2/CO_2$/d mixtures obtained substituting all (44.6%) of the CO_2 content with d = N_2, He, and Ar (RUN 15–18).

[Color figure can be viewed in the online issue, which is available at wileyonlinelibrary.com.]

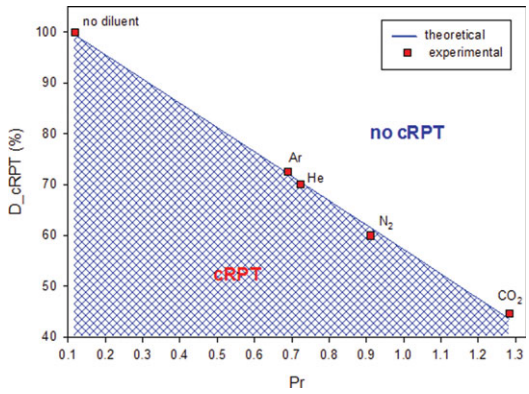

Figure 13. D_cRPT limits for different diluents.

[Color figure can be viewed in the online issue, which is available at wileyonlinelibrary.com.]

$$\text{D\_cRPT} = (2.19 - Pr)/0.0208 \quad (11)$$

The nature of the diluent affects the *Nu* number through the *Pr* number, thus modifying the thermal boundary layer. The D_cRPT limit increases as the *Pr* number decreases (Eq. 11). This means that the region of existence for the cRPT phenomenon reduces as the thermal boundary layer decreases.

Discussion of the Results

In all the pressure–time histories that show the cRPT peak, the signal is oscillating. Furthermore, the period of the oscillations changes. We calculated the period of the oscillations in the three phases (T_I, T_II, and T_III) for all runs that exhibit the cRPT phenomenon. In Table 3, the values of the dominant period of the oscillations computed in the three phases (Figure 3) are given. They were calculated by means of the FFT analysis. These values can be compared and related to the time constants and to their ratios (θ_1 and θ_2; Table 3). In particular, in Figure 14, the period of the oscillations computed for phase II (which includes the overadiabatic pressure peak) is plotted vs. the ratio between the time of condensation by cooling of the water in the gas phase and the time of evaporation of the water at the walls (by radiation; $\theta_2 = \tau_{cond}/\tau_{rad}$). The period increases with θ_2, meaning that the oscillations occurring during phase II are the result of the competition between evaporation (τ_{rad}) and condensation (τ_{cond}) of the water at the vessel walls.

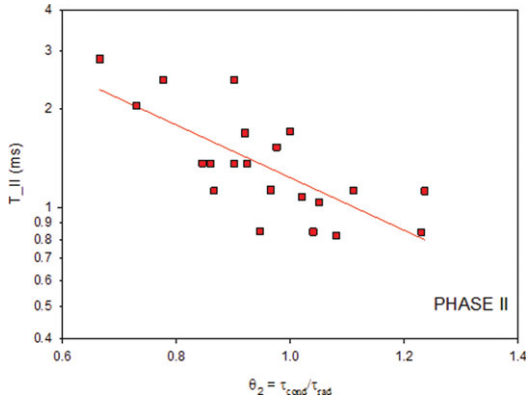

Figure 14. Period of the oscillations computed for phase II as a function of the ratio between the condensation time and the radiation time (all runs that exhibit the cRPT phenomenon).

[Color figure can be viewed in the online issue, which is available at wileyonlinelibrary.com.]

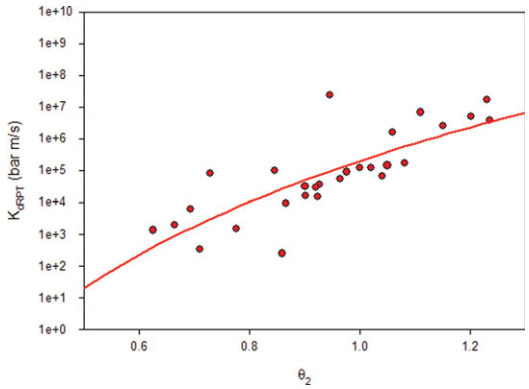

Figure 15. cRPT deflagration index (K_{cRPT}) vs. θ_2 (all runs that exhibit the cRPT phenomenon).

[Color figure can be viewed in the online issue, which is available at wileyonlinelibrary.com.]

In Figure 15, the cRPT deflagration index (K_{cRPT}) is plotted vs. θ_2 for all runs in which the cRPT phenomenon is observed. The figure shows that K_{cRPT} is well correlated to θ_2.

From Table 3, it can be seen that the cRPT phenomenon arises when θ_1 (i.e., the ratio between the condensation time, τ_{cond}, and the time for radial flame propagation, τ_{reac}) is higher than 1. This suggests that the oscillating behavior establishes when the reaction rate is faster than the condensation rate. Under these conditions, during reaction, water is produced and slowly condenses at the walls. In Figure 16, a zoom of the oscillations for phase I of RUN 3 is shown.

The oscillating behavior is activated by the competition between two phenomena: starting from point A, the pressure increases up to point B due to the combustion reaction. In going from A to B, water is produced and the bulk gas temperature and the water partial pressure increase. As a result, water condensates at the cold walls of the vessel, leading to bulk gas temperature and water partial pressure decrease and then the pressure shifts from point B to point C. The water condensation is balanced by the water production by reaction, thus leading to an increase of the water partial pressure. Then the cycle starts again.

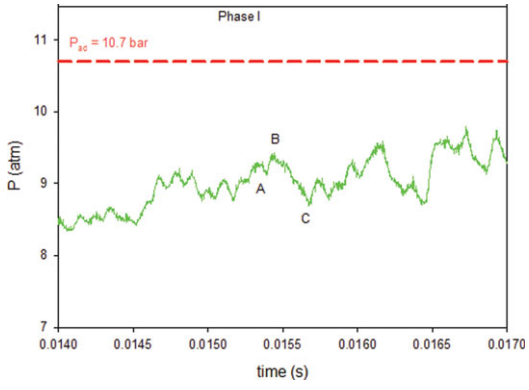

Figure 16. Oscillation wave in phase I (RUN 3).

[Color figure can be viewed in the online issue, which is available at wileyonlinelibrary.com.]

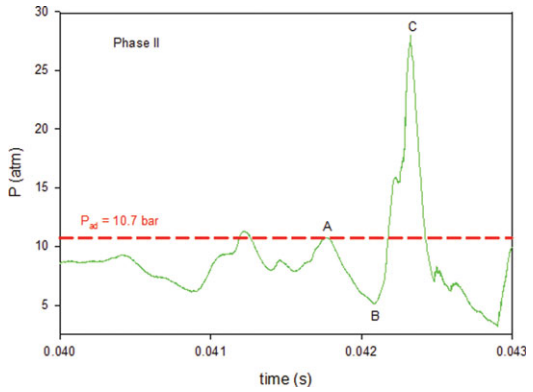

Figure 17. Oscillation wave in phase II (RUN 3).

[Color figure can be viewed in the online issue, which is available at wileyonlinelibrary.com.]

The oscillating phenomenon is then driven by the evaporation/condensation of water in the boundary layer, which is activated by the heat transfer between the vessel walls and the bulk gas phase and by variations in the water partial pressure occurring in the bulk. These phenomena significantly affect the nature of the boundary layer.

Conversely, when the radial flame propagation rate is lower than the condensation rate ($\theta_1 < 1$), the water condensates at the walls as soon as it is formed and the bulk gas temperature decreases: the slow reaction is not able to compensate the pressure decrease due to water condensation.

In the second phase, pressure peaks higher than the adiabatic values are observed. In Figure 17, a zoom of the pressure history for phase II of RUN 3 is shown.

The adiabatic pressure ($P_{ad} = 10.7$ bar) is also reported. Three peaks higher than the adiabatic values are found. Comparing the period of the oscillations with the ratio between the radiation time and the condensation time (θ_2), we may conclude that the synchronization between flame radiation and water condensation leads to the occurrence of the oscillations. In phase II, the reaction is completed. Starting from point A, a pressure decrease is observed due to heat losses and water condensation at the vessel walls (point B). Because of heat transfer from the burned gas, the water at the walls starts overheating up to reach the superheating temperature ($T_{sh} = 0.8 \cdot 374°C \approx 299°C$). At this temperature, the water evaporation occurs explosively,[2] generating shock waves: the pressure signal reaches point C which is overadiabatic. From point C, the pressure decreases owing to water condensation and the cycle starts again. In the vessel, superheating is achieved because the vessel walls and the liquid water produced by combustion are free of nucleation sites.

Conclusions

The effect of CO_2, N_2, He, and Ar addition on the c-RPT of CH_4/O_2 stoichiometric mixtures has been explored.

In all the conditions, the violence of the cRPT phenomenon is dominated by the ratio between the time of water rapid phase transition through radiative heat flux and the time of water condensation through cooling at the walls.

The limit values of the diluent concentration at which the cRPT phenomenon is suppressed have been found and correlated to the kinematic viscosity and the thermal diffusivity through the Prandtl number.

The less effective diluent has been found to be Ar followed by He, N_2, and CO_2 in the order listed.

Literature Cited

1. Di Benedetto A, Cammarota F, Di Sarli V, Salzano E, Russo G. Anomalous behavior during explosions of CH_4 in oxygen-enriched air. *Combust Flame*. 2011;158:2214–2219.
2. Reid RC. Superheated liquids. *Am Sci*. 1976;64:146–156.
3. Moore GR. Vaporization of superheated drops in liquids. Ph.D. Thesis, University of Wisconsin, 1956.
4. Wakeshima H, Takata K. On the limit of superheat. *J Phys Soc Jpn*. 1958;13:1398–1403.
5. Blander M, Kratz JL. Bubble nucleation in liquids. *AIChE J*. 1975;21:833–848.
6. Reid RC. Rapid phase transitions from liquid to vapor. *Adv Chem Eng*. 1983;12:105–208.
7. Nguyen VT, Furzeland RM, Ijpelaar JM. Rapid evaporation at the superheat limit. *Int J Heat Mass Transfer*. 1988;31:1687–1700.
8. McCann H, Clarke LJ, Masters AP. An experimental study of vapour growth at the superheat limit temperature. *Int J Heat Mass Transfer*. 1989;32:1077–1093.
9. Atallah S. Rapid phase transitions. Topical Report GRI-92/0533, Gas Research Institute, 1997.
10. Nedelka D, Sauter V, Goanvic J, Ohba R. Last developments in rapid phase transition knowledge and modeling techniques. Offshore Technology Conference, Houston, TX, Paper Number 15228-MS, 2003.
11. Reid RC. Possible mechanism for pressurized-liquid tank explosion or BLEVE's. *Science*. 1979;203:1263–1265.
12. Corradini ML, Kim BJ, Oh MD. Vapor explosions in light water reactors: a review of theory and modeling. *Prog Nucl Energy*. 1988;22:1–117.
13. Hess PD, Brondyke KJ. Causes of molten aluminum-water explosions and their prevention. *Met Prog*. 1969;95:93–100.
14. Epstein M, Fauske HK, Theofanous TG. On the mechanism of aluminum ignition in steam explosions. *Nucl Eng Des*. 2000;201:71–82.
15. Corradini ML, Swenson DV, Woodfin RL, Voelker LE. An analysis of containment failure by a steam explosion following a postulated core meltdown in a light water reactor. *Nucl Eng Des*. 1981;66:287–298.
16. Freundt A. Entrance of hot pyroclastic flows into the sea: experimental observations. *Bull Volcanol*. 2003;65:144–164.
17. Schildberg HP, Holtappels K. *The course of explosions of $CH_4/O_2/N_2$-mixtures in a 20 l sphere. Proceedings of the 13th International Symposium on Loss Prevention*, Brugge, Belgium, 2010.
18. Schildberg HP. The course of the explosions of combustible/O_2/N_2 mixtures in vessel-like geometry. *Forsch Ingenieurwes*. 2009;73:33–65.
19. Di Benedetto A, Di Sarli V, Salzano E, Cammarota F, Russo G. Explosion behavior of $CH_4/O_2/N_2/CO_2$ and $H_2/O_2/N_2/CO_2$ mixtures. *Int J Hydrogen Energy*. 2009;34:6970–6978.
20. Incropera FP, DeWitt DP. *Fundamentals of Heat and Mass Transfer*, 4th ed. New York: Wiley, 1996.
21. Kee RJ, Grcar JF, Smooke MD, Miller JA. *A FORTRAN program for modeling steady laminar one-dimensional premixed flames*. Sandia National Laboratories Report, SAND 85–8240, 1985.
22. Leckner B. Spectral and total emissivity of water vapor and carbon dioxide. *Combust Flame*. 1972;19:33–48.
23. Bowman CT, Frenklach M, Gardiner WC, Smith GP. *The "GRI-Mech 3.0" Chemical Kinetic Mechanism*. 1999. Available at: www.me.berkeley.edu/grimech/.

Manuscript received July 4, 2011, and revision received Sept. 6, 2011.